

Kondo physics versus spin-gap physics in fully spin-split quantum wires

F. Sfigakis,* C.J.B. Ford, M. Pepper,† D. A. Ritchie, I. Farrer, and M. Y. Simmons‡
Cavendish Laboratory, J. J. Thomson Avenue, Cambridge, CB3 0HE, United Kingdom

D. Maude

Grenoble High Magnetic Field Laboratory, 25 avenue des Martyrs, Grenoble, BP 166, France

Linear and nonlinear transport of quantum wires are investigated at a magnetic field where spin-split one-dimensional (1D) subbands are equidistant in energy. In this seldom-studied regime, experiments are consistent with a density-dependent energy gap between spin subbands, and with a complete spin polarization of the first 1D subband under a large source-drain bias at zero field.

PACS numbers: 73.63.Nm, 72.25.Dc, 73.21.Hb, 73.23.Ad

Using split-gate devices,¹ the quantization of the differential conductance $G = dI/dV_{sd}$ in units of $G_0 = 2e^2/h$ in ballistic quantum wires^{2,3} is well understood in terms of non-interacting electrons. However, a conductance feature near $\sim 0.7 G_0$, the so-called 0.7 anomaly or 0.7 structure,⁴ cannot be explained in such terms. The discovery of “0.7 analogs” at Zeeman crossings,⁵ where Zeeman-split 1D subbands of opposite spins become degenerate in energy, initially suggested that the physical mechanism of the 0.7 structure becomes manifest whenever two levels of opposite spin become degenerate in energy. Despite considerable attention, both theoretical and experimental, the physical origins of the 0.7 structure/analog are still unclear. Models based on spin polarization^{6,7,8,9,10,11,12,13,14,15,16,17,18,19,20,21,22,23,24,25,26,27,28} (with an energy gap, also referred to as a “spin gap”, opening between spin-split subbands) and on Kondo physics^{29,30,31,32,33,34,35,36,37,38,39} (involving a quasi-bound state in the 1D channel) can describe most – but not all – of the phenomenology associated with the 0.7 structure/analog. For example, spin polarization models do not predict the occurrence of a zero-bias anomaly in quantum wires,⁴⁰ whilst Kondo physics models do not describe well the 0.85 plateau at high source-drain bias.⁴¹ Also, in many experiments, one cannot resolve which model best fits the data. For example, the shot noise suppression near the 0.7 structure can be described by either models,^{19,35} and the temperature dependence of the 0.7 structure can be described by either an exponential⁹ or a power law.³⁰ There is thus a need for experiments that can unambiguously point to one (or neither!) type of models.

Transport in an in-plane magnetic field $B = B_1$ [see inset of Fig. 1(a)], where spin-split 1D subbands are equidistant in energy (B_1 is halfway between $B = 0$ and the Zeeman crossing at $B = B_2$), allows the properties of spin \downarrow (defined as the spin type lowest in energy at finite B) and spin \uparrow subbands to be studied *separately*. In this article, we demonstrate that many-body effects are not restricted merely to regimes of near-degeneracy between electrons of opposite spin. Our experimental results are not consistent with Kondo physics or purely pinning^{8,12} of the spin \uparrow subband near a chemical potential. Our

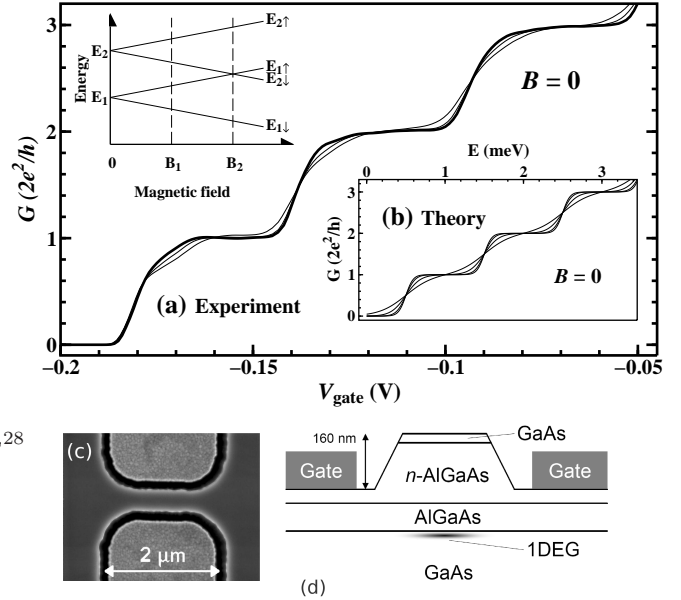


FIG. 1: (a) Measured conductance of sample A at $B = 0$ for $T = 0.3$ K (thickest trace), 0.6 K, and 1 K. (INSET) Energy diagram depicting the Zeeman effect on the first two 1D subbands. At B_1 , the spin subbands are fully spin-split; at B_2 , the $E_{\ell\uparrow}$ and $E_{(\ell+1)\downarrow}$ energy levels are degenerate (a “Zeeman crossing”). (b) Calculated conductance using Eqs. (1)–(3) with $\omega_y/\omega_x = 4$, $\hbar\omega_y = 1$ meV, and $k_B T = 0.02$ meV (thickest trace), 0.04 meV, 0.08 meV, and 0.16 meV. In a saddle point potential, conductance quantisation is completely lost when $\hbar\omega_y = 4k_B T$. (c) Scanning electron microscope (SEM) image of sample A. (d) Schematic view of the cross-section of the quantum wire shown in (c).

experimental data is consistent to spin-gap models based on the concept of a spin gap affecting *both* spin \uparrow and spin \downarrow subbands.

Samples (A, B, C) were fabricated from three GaAs/AlGaAs single heterojunction 2D electron gases (all ~ 300 nm deep) with carrier densities of $(1.26, 1.82, 0.94) \times 10^{15} \text{ m}^{-2}$ and mobilities of $(355, 475, 195) \text{ m}^2/\text{Vs}$, whose Molecular Beam Epitaxy (MBE) layer structure is (from the top): a 17 nm GaAs cap, a (215, 215, 200) nm n-doped (Si) $\text{Al}_{0.33}\text{Ga}_{0.67}\text{As}$ doped layer,

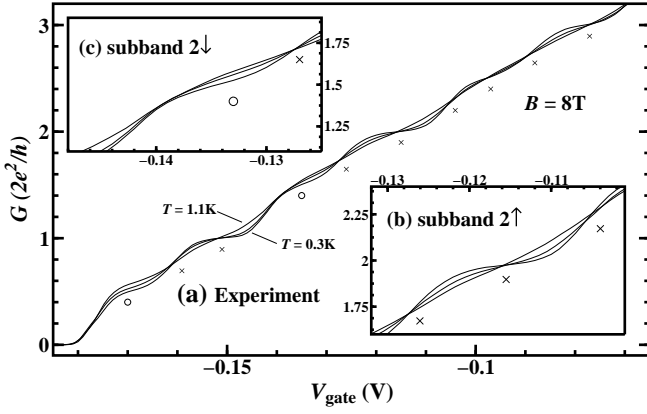


FIG. 2: (a) Measured conductance of sample A at $B = 8.0$ T where spin subbands are almost fully spin-split, for $T = 0.3$ K, 0.6 K, and 1.1 K. Enlarged view of: (b) the integer $2.0 G_0$ plateau, and (c) the half-integer $1.5 G_0$ plateau. The ‘x’ and ‘o’ symbols are explained in the main text.

a (70, 70, 80) nm undoped $\text{Al}_{0.33}\text{Ga}_{0.67}\text{As}$ spacer layer, and 500 nm semi-insulating GaAs. Self-aligned recessed metal gates were evaporated after a 160 nm deep etch, using a 1:1:38 $\text{H}_3\text{PO}_4:\text{H}_2\text{O}_2:\text{H}_2\text{O}$ solution (by volume), shown in Figs. 1(c)-1(d). The etched 1D channels for samples (A, B, C) were (0.75, 0.02, 0.02) μm long and 0.35–0.40 μm wide. Their differential conductance was measured in dilution refrigerators (with 0.04 K and 0.3 K base electron temperatures), using standard lock-in techniques.

Figure 1(a) shows a “classic” 0.7 structure in sample A as the temperature T is increased. Note the T -invariant points at $G/G_0 = 1, 1.5, 2, 2.5,$ and 3 . In an attempt to gain some physical insight, we used a “toy model” to calculate conductance; it is not meant to exactly reproduce experimental data, but rather illustrate types of behavior. Using a saddle-point potential,⁴⁷ we calculate the 1D conductance at equilibrium with:

$$G(\mu, T, B) = \frac{e^2}{h} \sum_{\ell=0} \sum_{\varsigma=\uparrow,\downarrow} \int_0^\infty \left[T_{\ell\varsigma}(E) \right] \times \left[-\frac{\partial f}{\partial E}(E, \mu, T) \right] dE \quad (1)$$

where $T_{\ell\varsigma}(E) = [1 + e^{-2\pi(E-E_{\ell\varsigma})/\hbar\omega_x}]^{-1}$ is the transmission coefficient for each spin subband, $E_{\ell\varsigma}$ are given by

$$E_{\ell\downarrow} = \hbar\omega_y(\ell + \frac{1}{2}) - \frac{1}{2}|g|\mu_B B \quad (2)$$

$$E_{\ell\uparrow} = \hbar\omega_y(\ell + \frac{1}{2}) + \frac{1}{2}|g|\mu_B B, \quad (3)$$

ς labels the spin type (\uparrow, \downarrow), ℓ the 1D subband index, μ is the equilibrium chemical potential, k_B the Boltzmann constant, $-\frac{\partial f}{\partial E}(E, \mu, T) = [4k_B T \cosh^2[(E - \mu)/2k_B T]]^{-1}$ the derivative of the Fermi function, $\hbar\omega_x$ the energy broadening due to quantum tunneling, $\hbar\omega_y$ the 1D subband energy level spacing, g the bulk GaAs Landé g -factor ($|g| = 0.44$), and μ_B the Bohr magneton. In

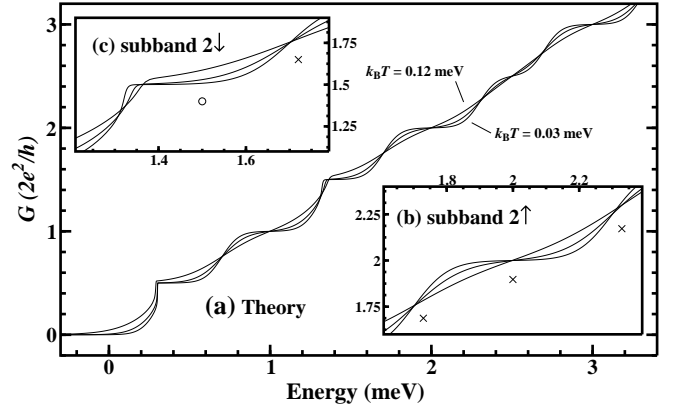


FIG. 3: (a) Simulated conductance at $|g|\mu_B B/\hbar\omega_y = 0.4$, using Eqs.(1)–(5) with $\gamma_0 = 60$, $\gamma_1 = 30$, and $\gamma_2 = 0 \mu\text{eV}\cdot\mu\text{m}^2$, $\omega_y/\omega_x = 4$, $\hbar\omega_y = 1$ meV, $r = 2$, and $k_B T = 0.03, 0.06,$ and 0.12 meV. Enlarged view of: (b) the integer $2.0 G_0$ plateau, and (c) the half-integer $1.5 G_0$ plateau.

both calculations and experiments, magnetic field B is in-plane, along the current flow through the 1D channel in the x -direction. The y -direction is in-plane, perpendicular to the current flow, and the z -direction is out of the plane. For simplicity, the effects of diamagnetic shift^{48,49,50} have been omitted. Provided the pinch-off voltage does not drift with time⁵¹ and the 1D constriction can be described by a saddle-point potential, T -invariant points should occur either (i) at mid-height of a riser whenever a subband energy level $E_{\ell\varsigma}$ crosses μ , or (ii) at mid-length of a plateau whenever μ is exactly halfway between two subband energy levels. Comparing Figs. 1(a) with 1(b), the conductance G behaves mostly as predicted by Eq. (1) for $G \geq 2e^2/h$. The same observations apply to split-gated samples, e.g. see Figure 1(a) in Ref. 30 and Figure 4 in Ref. 4.

Figure 2 shows the (constant-voltage) four-terminal conductance of sample A for the first six almost fully spin-split plateaus ($B \lesssim B_1$). The riser of each quantized plateau is due to the population of the $1\downarrow, 1\uparrow, 2\downarrow, 2\uparrow, 3\downarrow,$ and $3\uparrow$ spin subbands, in that order. The measured conductance has many T -invariant points (indicated by a ‘x’), as predicted by Eq. (1). However, there are none at mid-length of the $0.5 G_0$ and $1.5 G_0$ quantized plateaus: as T increases, almost all of the plateau rises in conductance (indicated by an ‘o’). This has been previously observed in split-gated samples,^{5,52} but only for the spin-split $0.5 G_0$ plateau and no mechanism was proposed. If $|g|\mu_B B < 4k_B T < 2\hbar\omega_y$ in the regime $0 < B < B_1$, Eq. (1) predicts the T -invariant points at $0.5, 1.0, 1.5, 2.0, 2.5,$ and $3.0 G_0$ always remain visible whilst those at $0.75, 1.75,$ and $2.75 G_0$ only disappear if $\hbar\omega_y < 4k_B T$. Clearly, the latter T -invariant points are still present in Figure 2 at all temperatures: the observed thermal broadening involves at most only one spin subband at mid-height of each riser, or at most only two spin subbands on the middle of each plateau. Furthermore, the $2.5 G_0$ plateau

behaves as expected from non-interacting electrons, with a T -invariant point at $2.5G_0$. The rise of the $1.5G_0$ and $0.5G_0$ plateaus above their nominal quantized value with increasing temperature cannot be explained within a single-particle picture.

At $B = 0$, the rise of the 0.7 structure to $G_0 = 2e^2/h$ with decreasing temperature has been suggested to result from Kondo physics.³⁰ At $B = 8$ T, the behavior of the $0.5G_0$ and $1.5G_0$ plateaus in Fig. 2 cannot be attributed either to Kondo physics: the experimental G rises with increasing T (the opposite temperature dependence is predicted^{31,43}). Furthermore, the Kondo effect is completely suppressed in large magnetic fields (far away from spin degeneracy points at $B = 0$ and $B = B_2$), such as when the spin-split $0.5G_0$ plateau appears. Pinning alone of the spin \uparrow subbands to the chemical potential⁸ also cannot explain the behaviour of the $0.5G_0$ and $1.5G_0$ plateaus associated with populating spin \downarrow subbands. However, the behavior shown in Figure 2 could be consistent with a density-dependent spin gap opening between spin subbands.

To illustrate this, we calculated the conductance using Eq. (1), but with $E_{\ell\downarrow}$ redefined as (valid only if $B \approx B_1$, see further below):

$$E_{\ell\downarrow} \approx \hbar\omega_y(\ell + \frac{1}{2}) - \gamma_\ell(n_{\ell\downarrow} + n_{\ell\uparrow})^r \quad (4)$$

where $(n_{\ell\downarrow} + n_{\ell\uparrow})$ is the electron density of 1D subband ℓ (per unit length along the 1D channel) and γ_ℓ is the electron-electron interaction strength in subband ℓ . The individual subband densities $n_{\ell\zeta}$ are calculated using:

$$n_{\ell\zeta} = \int_{E_{\ell\zeta}}^{\infty} g_{1D}(E, E_{\ell\zeta}) f(E, \mu, T) dE \quad (5)$$

where $g_{1D}(E, E_{\ell\zeta}) = \sqrt{2m^*}(2\pi\hbar\sqrt{E - E_{\ell\zeta}})^{-1}$ is the 1D density of states. All variables $E_{\ell\zeta}$ and $n_{\ell\zeta}$ were calculated self-consistently. It is unlikely that a spin gap occurring in real samples increases indefinitely with increasing electron density: it must eventually either saturate or close.^{6,20} However, when $E_{\ell\downarrow}$ is deep below μ , the $\ell\downarrow$ spin subband contributes e^2/h to the total conductance, regardless of whether the spin gap is open or closed. Therefore, for simplicity, we did not include any term in Eq. (4) to ensure that the spin gap eventually closes or saturates. At $B = 0$ or near Zeeman crossings ($B \approx B_2$), in many spin-gap models, the apparent ‘‘pinning’’ of $E_{\ell\uparrow}$ near a chemical potential is thought responsible for the appearance of the 0.7 structure/analogs. However, our data (Figs. 2 and 4) do not show unusual behavior associated with $E_{\ell\uparrow}$ when $B \approx B_1$: either $E_{\ell\uparrow}$ is far enough above μ to contribute very little to the total conductance regardless of any spin gap, or the spin gap must have already closed or saturated when $E_{\ell\uparrow}$ crosses μ . Again for simplicity, we used Eq. (3) to describe $E_{\ell\uparrow}$. These simplifying approximations are only valid if $B \approx B_1$.

The magnetic field in Figure 3 is $|g|\mu_B B/\hbar\omega_y = 0.4$ (note $B \equiv B_1$ if $|g|\mu_B B/\hbar\omega_y = \frac{1}{2}$) to be closer to the

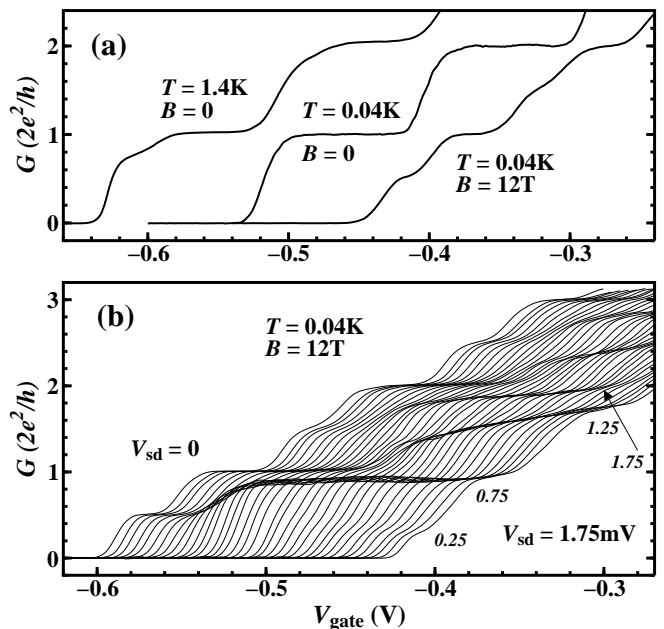


FIG. 4: (a) Measured conductance at equilibrium of sample B in three different regimes (traces offset laterally). (b) Non-equilibrium conductance in magnetic field from $V_{sd} = 0$ to $V_{sd} = +1.75$ mV in 0.05 mV steps (traces offset laterally). Note the evolution from half-integer plateaus to quarter-integer plateaus as V_{sd} increases.

experimental situation in Figure 2. The simulated $0.5G_0$ and $1.5G_0$ half-integer plateaus rise above their nominal value, while all other plateaus behave as expected from a single-particle picture. The exact functional form of the opening spin gap is not critical: similar behavior was also obtained for simulations with $r = \frac{1}{2}$ and $r = 1$. The key here is that spin \downarrow subbands populate much more rapidly below the chemical potential than spin \uparrow subbands.

Figure 4(a) shows a ‘‘classic’’ 0.7 structure at 1.4 K in sample B, with a clean $2e^2/h$ plateau at 0.04 K. Although $B_1 > 12$ T, the 1D subbands are clearly spin-split. Figure 4(b) shows conductance traces under increasing V_{sd} at $B = 12$ T, where so-called ‘‘quarter-integer’’ plateaus^{53,54} are observed. For subband $\ell = 2$, the $2.75G_0$ and $2.25G_0$ quarter-integer plateaus are easily identifiable, with the latter appearing at a slightly larger V_{sd} than the $2.75G_0$ plateau. For subband $\ell = 1$, the $1.75G_0$ plateau has almost fully formed while the $1.25G_0$ plateau has only begun to form. For subband $\ell = 0$, the trend continues with a very well defined plateau at $\sim 0.8G_0$ but with no signs of a $0.25G_0$ plateau until a very large V_{sd} is applied. Identical behavior occurs for $V_{sd} < 0$ (not shown). In high-indexed plateaus ($\ell \geq 4$) where one expects electron-electron interactions to be minimal, both the $(\ell + 0.25)G_0$ and $(\ell + 0.75)G_0$ plateaus appear at the *same* V_{sd} (not shown). Kondo physics cannot account for this behavior. However, the behavior shown in Figure 4 could be consistent with a density-dependent spin gap opening between spin subbands.

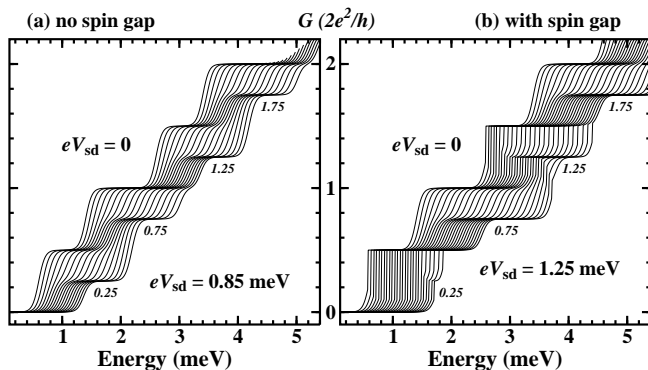


FIG. 5: Simulated conductance traces using Eq.(6) for a fixed V_{sd} at $k_B T = 5 \mu\text{eV}$ and $|g|\mu_B B = 0.4\hbar\omega_y$ for a 1D channel with $\omega_y/\omega_x = 4$ and $\hbar\omega_y = 2 \text{ meV}$ in two situations: (a) non-interacting electrons, and (b) interacting electrons. Source-drain bias V_{sd} is increased in 0.05 meV steps from left to right (traces offset laterally). Note the late onset of the $0.25 G_0$ and $1.25 G_0$ quarter-integer plateaus in (b) compared to (a). Parameters used in the calculations were $r = 1$, $\gamma_0 = 150 \mu\text{eV}\cdot\mu\text{m}$, $\gamma_1 = 75 \mu\text{eV}\cdot\mu\text{m}$, and $\gamma_2 = 0$. Variables $E_{\ell\zeta}$ and $n_{\ell\zeta}$ were calculated self-consistently using Eqs. (4)–(5).

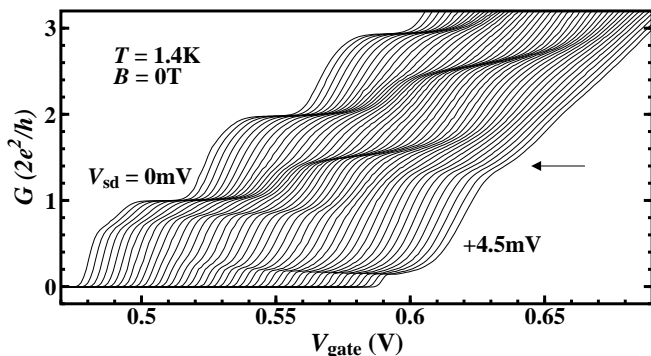


FIG. 6: Measured conductance of sample C at $B = 0\text{T}$ (traces offset laterally) from $V_{sd} = 0$ (leftmost) to $V_{sd} = +4.5 \text{ mV}$ (rightmost) in 0.1 mV steps. Note how the $\sim 0.8 G_0$ and the $\sim 0.3 G_0$ plateaus look nearly identical to the $0.75 G_0$ and $0.25 G_0$ plateaus of Figure 4(b), except for the presence of the $0.5 G_0$ plateau near $V_{sd} = 0$.

Applying the Glazman-Khaetskii formalism⁵⁵ to Eq. (1), the non-equilibrium 1D conductance becomes:

$$G(\mu, T, B, V_{sd}) = \frac{e^2}{h} \sum_{\ell=0} \sum_{\zeta=\uparrow,\downarrow} \int_0^\infty \left[-\frac{\partial f}{\partial E}(E, \mu, T) \right] \times \frac{1}{2} \left[T_{\ell\zeta}(\mu_s) + T_{\ell\zeta}(\mu_d) \right] dE \quad (6)$$

where $\mu_s = E + \frac{1}{2}eV_{sd}$ and $\mu_d = E - \frac{1}{2}eV_{sd}$ are the chemical potentials at source and drain respectively. Figure 5(a) shows calculated non-equilibrium conductance traces for non-interacting electrons at a fixed magnetic field. Since $|g|\mu_B B/\hbar\omega_y < \frac{1}{2}$, the spin-split half-integer plateaus dis-

appear before the integer plateaus (as in the experimental data). Note how the onsets of the $(\ell + 0.25) G_0$ and $(\ell + 0.75) G_0$ quarter-integer plateaus appear at the *same* V_{sd} . By contrast, with a spin gap, Figure 5(b) shows that the $0.25 G_0$ and $1.25 G_0$ plateaus appear at a much *higher* V_{sd} than their $0.75 G_0$ and $1.75 G_0$ counterparts (as in the experimental data). Essentially, the $(\ell + 0.25) G_0$ plateau can only form once eV_{sd} exceeds the spin-gap energy $\gamma_\ell(n_{\ell\downarrow} + n_{\ell\uparrow})^r$ of the $\ell\downarrow$ spin subband.

It is interesting to compare Figures 4 and 5 with Figure 6, showing the effect of a finite V_{sd} on sample C at $B = 0$. For $G > 2e^2/h$, plateaus at half-integer multiples of G_0 appear,⁵⁶ as expected in a single-particle picture. For $G < 2e^2/h$, plateaus are observed at $0.8\text{--}0.9 G_0$ and $0.2\text{--}0.3 G_0$, which have often been assigned the values $0.85 G_0$ and $0.50 G_0$ in the literature.^{9,30,57} These have been shown not to be associated with Kondo physics in samples where a bound state was deliberately engineered to form in the 1D channel.⁴¹ Here, we essentially reproduce the same result in clean quantum wires (of which sample C is representative). Furthermore, the zero-field $0.8\text{--}0.9 G_0$ and $0.2\text{--}0.3 G_0$ plateaus do not show any signs of splitting as B is increased,^{54,58} leading us to interpret them as zero-field quarter-integer plateaus, nominally at $0.75 G_0$ and $0.25 G_0$.^{26,28} This would be consistent with the simulations of Fig. 5(b), where the spin-gap energy, $\gamma_\ell(n_{\ell\downarrow} + n_{\ell\uparrow})^r$, increases with increasing source-drain bias V_{sd} .

Consequently to the reasoning above, the plateau near $\sim 1.4 G_0$ at the highest V_{sd} in Fig. 6 (see arrow), also reported in Refs. 9 and 15, should be the $1.25 G_0$ quarter-integer plateau. Unambiguous identification of plateaus at finite V_{sd} has always been difficult because of the rise in G with increasing V_{sd} . This rise can be described by “self-gating”,⁹ a single electron effect.

In conclusion, we have presented data showing interacting electron effects in finite magnetic fields, far away from near-degeneracy points between spin-split subbands, consistent with the existence of a spin gap and inconsistent with Kondo physics. We have also demonstrated, in a clean quantum wire, that the so-called $0.85 G_0$ plateau does not result from the suppression of a Kondo-enhanced conductance from the $2e^2/h$ plateau, but is rather a fully spin-split plateau. Within a spin-gap interpretation of the 0.7 structure, our results strongly suggest that spin \downarrow subbands are also affected by the spin gap, a mechanism that had not been made experimentally evident until now. Finally, we propose to use quantum wires under a large source-drain bias (in a regime where the $0.25 G_0$ plateau becomes visible) to produce a uni-directional, spin-polarised current.

We thank A.C. Graham, V. Tripathi, T.-M. Chen, K.-F. Berggren, and K. J. Thomas for insightful discussions, and K. Cooper, A. Beckett, R. Milanole and L. Lozano for technical assistance. This work was supported by the EPSRC (UK).

- * corresponding author: fs228@cam.ac.uk
- † Present address: Department of Electronic and Electrical Engineering, University College, London, WC1E 6BT, UK.
- ‡ Present address: School of Physics, University of New South Wales, Sydney 2052, Australia.
- ¹ T. J. Thornton, M. Pepper, H. Ahmed, D. Andrews, and G. J. Davies, *Phys. Rev. Lett.* **56**, 1198 (1986).
 - ² D. A. Wharam, T. J. Thornton, R. Newbury, M. Pepper, H. Ahmed, J. E. F. Frost, D. G. Hasko, D. C. Peacock, D. A. Ritchie, and G. A. C. Jones, *J. Phys. C* **21**, L209 (1988).
 - ³ B. J. van Wees, H. van Houten, C. W. J. Beenaker, J. G. Williamson, L. P. Kouwenhoven, D. van der Marel, and C. T. Foxon, *Phys. Rev. Lett.* **60**, 848 (1988).
 - ⁴ K. J. Thomas, J. T. Nicholls, M. Y. Simmons, M. Pepper, D. R. Mace, and D. A. Ritchie, *Phys. Rev. Lett.* **77**, 135 (1996).
 - ⁵ A. C. Graham, K. J. Thomas, M. Pepper, N. R. Cooper, M. Y. Simmons, and D. A. Ritchie, *Phys. Rev. Lett.* **91**, 136404 (2003).
 - ⁶ C. K. Wang and K. F. Berggren, *Phys. Rev. B* **54**, R14257 (1996).
 - ⁷ K. J. Thomas, J. T. Nicholls, N. J. Appleyard, M. Y. Simmons, M. Pepper, D. R. Mace, W. R. Tribe, and D. A. Ritchie, *Phys. Rev. B* **58**, 4846 (1998).
 - ⁸ S. Nuttinck, K. Hashimoto, S. Miyashita, T. Saku, Y. Yamamoto, and Y. Hirayama, *Jpn. J. Appl. Phys.* **39**, L655 (2000).
 - ⁹ A. Kristensen, H. Bruus, A. Hansen, J. B. Jensen, P. E. Lindelof, C. J. Marckmann, J. Nygard, and C. B. Sorensen, *Phys. Rev. B* **62**, 10950 (2000).
 - ¹⁰ N. J. Appleyard, J. T. Nicholls, M. Pepper, W. R. Tribe, M. Y. Simmons, and D. A. Ritchie, *Phys. Rev. B* **62**, R16275 (2000).
 - ¹¹ K. Hirose and N. S. Wingreen, *Phys. Rev. B* **64**, 073305 (2001).
 - ¹² A. Kristensen and H. Bruus, *Physica Scripta* **101**, 151 (2002).
 - ¹³ D. J. Reilly, T. M. Buehler, J. L. O'Brien, A. R. Hamilton, A. S. Dzurak, R. G. Clark, B. E. Kane, L. N. Pfeiffer, and K. W. West, *Phys. Rev. Lett.* **89**, 246801 (2002).
 - ¹⁴ P. Havu, M. J. Puska, R. M. Nieminen, and V. Havu, *Phys. Rev. B* **70**, 233308 (2004).
 - ¹⁵ D. J. Reilly, *Phys. Rev. B* **72**, 033309 (2005).
 - ¹⁶ K. F. Berggren, P. Jaksch, and I. Yakimenko, *Phys. Rev. B* **71**, 115303 (2005).
 - ¹⁷ L. P. Rokhinson, L. N. Pfeiffer, and K. West, *Phys. Rev. Lett.* **96**, 156602 (2006).
 - ¹⁸ O. Chiatti, J. T. Nicholls, Y. Proskuryakov, N. Lumpkin, I. Farrer, and D. A. Ritchie, *Phys. Rev. Lett.* **97**, 056601 (2006).
 - ¹⁹ L. DiCarlo, Y. Zhang, D. T. McClure, D. J. Reilly, C. M. Marcus, L. N. Pfeiffer, and K. West, *Phys. Rev. Lett.* **97**, 036810 (2006).
 - ²⁰ P. Jaksch, I. Yakimenko, and K. F. Berggren, *Phys. Rev. B* **74**, 235320 (2006).
 - ²¹ A. Lassel, P. Schlagheck, , and K. Richter, *Phys. Rev. B* **75**, 045346 (2007).
 - ²² A. C. Graham, D. L. Sawkey, M. Pepper, M. Y. Simmons, and D. A. Ritchie, *Phys. Rev. B* **75**, 035331 (2007).
 - ²³ E. J. Koop, A. I. Lerescu, J. Liu, B. J. vanWees, D. Reuter, A. D. Wieck, and C. H. van der Wal, *J. Supercond. Nov. Magn.* **20**, 433 (2007).
 - ²⁴ K. F. Berggren and I. Yakimenko, *J. Phys.: Condens. Matter* **20**, 164203 (2008).
 - ²⁵ A. C. Graham, M. Y. Simmons, D. A. Ritchie, and M. Pepper, *Phys. Rev. Lett.* **100**, 226804 (2008).
 - ²⁶ T.-M. Chen, A. C. Graham, M. Pepper, I. Farrer, and D. A. Ritchie, *Appl. Phys. Lett.* **93**, 032102 (2008).
 - ²⁷ T.-M. Chen, A. C. Graham, M. Pepper, F. Sfigakis, I. Farrer, , and D. A. Ritchie, *Phys. Rev. B* **79**, 081303(R) (2009).
 - ²⁸ P. J. Simmonds, F. Sfigakis, H. E. Beere, D. A. Ritchie, M. Pepper, D. Anderson, and G. A. C. Jones, *Appl. Phys. Lett.* **92**, 152108 (2008).
 - ²⁹ P. E. Lindelof, *Proc. SPIE Int. Soc. Opt. Eng.* **4415**, 77 (2001).
 - ³⁰ S. M. Cronenwett, H. J. Lynch, D. Goldhaber-Gordon, L. P. Kouwenhoven, C. M. Marcus, K. Hirose, N. S. Wingreen, and V. Umansky, *Phys. Rev. Lett.* **88**, 226805 (2002).
 - ³¹ Y. Meir, K. Hirose, and N. S. Wingreen, *Phys. Rev. Lett.* **89**, 196802 (2002).
 - ³² O. P. Sushkov, *Phys. Rev. B* **67**, 195318 (2003).
 - ³³ P. S. Cornaglia and C. A. Balseiro, *Europhys. Lett.* **67**, 634 (2004).
 - ³⁴ T. Rejec and Y. Meir, *Nature* **442**, 900 (2006).
 - ³⁵ A. Golub, T. Aono, and Y. Meir, *Phys. Rev. Lett.* **97**, 186801 (2006).
 - ³⁶ S. Luscher, L. S. Moore, T. Rejec, Y. Meir, H. Shtrikman, and D. Goldhaber-Gordon, *Phys. Rev. Lett.* **98**, 196805 (2007).
 - ³⁷ T. Aono, *Phys. Rev. B* **77**, 081303 (2008).
 - ³⁸ Y. Meir, *J. Phys.: Condens. Matter* **20**, 164208 (2008).
 - ³⁹ J. H. Jefferson, A. Ramsak, and T. Rejec, *J. Phys.: Condens. Matter* **20**, 164206 (2008).
 - ⁴⁰ S. Sarkozy, F. Sfigakis, K. D. Gupta, I. Farrer, D. A. Ritchie, G. A. C. Jones, and M. Pepper, *Phys. Rev. B* **79**, 161307(R) (2009).
 - ⁴¹ F. Sfigakis, C. J. B. Ford, M. Pepper, M. Kataoka, D. A. Ritchie, and M. Y. Simmons, *Phys. Rev. Lett.* **100**, 026807 (2008).
 - ⁴² K. A. Matveev, *Phys. Rev. Lett.* **92**, 106801 (2004).
 - ⁴³ K. A. Matveev, *Phys. Rev. B* **70**, 245319 (2004).
 - ⁴⁴ A. D. Klironomos, J. S. Meyer, T. Hikihara, and K. A. Matveev, *Phys. Rev. B* **76**, 075302 (2007).
 - ⁴⁵ G. A. Fiete, *Rev. Mod. Phys.* **79**, 801 (2007).
 - ⁴⁶ W. K. Hew, K. J. Thomas, M. Pepper, I. Farrer, D. Anderson, G. A. C. Jones, and D. A. Ritchie, *Phys. Rev. Lett.* **101**, 036801 (2008).
 - ⁴⁷ M. Buttiker, *Phys. Rev. B* **41**, 7906 (1990).
 - ⁴⁸ F. Stern, *Phys. Rev. Lett.* **21**, 1687 (1968).
 - ⁴⁹ B. Schuh, *J. Phys. A* **18**, 803 (1985).
 - ⁵⁰ G. Salis, T. Heinzel, K. Ensslin, O. J. Horman, W. Bachtold, K. Maranowski, and A. C. Gossard, *Phys. Rev. B* **60**, 7756 (1999).
 - ⁵¹ During a temperature dependence, one can easily diagnose drifting in time by comparing traces obtained whilst increasing and decreasing the temperature.
 - ⁵² K. J. Thomas, J. T. Nicholls, M. Y. Simmons, W. R. Tribe, A. G. Davies, and M. Pepper, *Physica E* **12**, 708 (2002).
 - ⁵³ N. K. Patel, J. T. Nicholls, L. Martin-Moreno, M. Pepper,

- J. E. F. Frost, D. A. Ritchie, and G. A. C. Jones, *Phys. Rev. B* **44**, 10973 (1991).
- ⁵⁴ K. J. Thomas, J. T. Nicholls, M. Y. Simmons, M. Pepper, D. R. Mace, and D. A. Ritchie, *Philos. Mag. B* **77**, 1213 (1998).
- ⁵⁵ L. I. Glazman and A. V. Khaetskii, *Europhys. Lett.* **9**, 263 (1989).
- ⁵⁶ N. K. Patel, J. T. Nicholls, L. Martin-Moreno, M. Pepper, J. E. F. Frost, D. A. Ritchie, and G. A. C. Jones, *Phys. Rev. B* **44**, 13549 (1991).
- ⁵⁷ D. J. Reilly, Y. Zhang, and L. DiCarlo, *Physica E* **34**, 27 (2006).
- ⁵⁸ A. C. Graham, M. Pepper, M. Y. Simmons, and D. Ritchie, *Physica E* **34**, 588 (2006).